Which number of b-value is better for accurate calculation of virtual MR elastography?

Poster No.:	C-1761
Congress:	ECR 2019
Type:	Scientific Exhibit
Authors:	Y. Matsumoto[1], M. Harada[2], Y. Kanazawa[2], M. Otomo[2], D. E. Amgalan[1], G. ariunbold[1], S. takamastu[3], Y. Yamashita[3]; [1]Tokushima-shi/JP, [2]Tokushima/JP, [3]Otawara-shi/JP
Keywords:	Technical aspects, Physics, MR-Diffusion/Perfusion, MR, Elastography, MR physics, Liver, Abdomen, Cirrhosis
DOI:	10.26044/ecr2019/C-1761

Aims and objectives

Shear stiffness is an important physical property of tissues and has been found to gradually increase with increasing hepatic fibrosis in chronic liver disease [1, 2]. In magnetic resonance imaging (MRI), it can be measured as image contrast by using magnetic resonance elastography (MRE), a technique that has been widely used to quantitatively assess shear stiffness for a diagnostic staging of hepatic fibrosis [1, 3, 4]. MRE is a completely non-invasive imaging technique, and the results can be easily interpreted in the clinic for molecular diagnosis of liver disease, without the need for liver biopsy.

Recently, virtual MRE has been reported by Le Behan et al [5]. Virtual MRE calculates the shear stiffness of the chronic liver disease from a physical consideration that amount of non-Gaussian diffusion empirically calculated from intravoxel incoherent motion (IVIM) signal attenuation relates the shear stiffness of tissue. There are several IVIM models to empirically detect the non-Gaussian diffusion [6-9]. For example, the amount of non-Gaussian diffusion in biological tissue can be detected by apparent diffusion coefficients (*ADCs*), which are slopes of signal attenuation for each of the slow and fast diffusion components [5]. In addition, *D** derived from the bi-exponential model also reflects the non-Gaussian diffusion [10]. Thus, there is the estimated parameter map which can represent the non-Gaussian diffusion in the IVIM model [11]. Moreover, the estimated parameter map derived from a curve fitted by IVIM model is varied depending on set b-value. Then, b-value would affect accurately calculating the shear stiffness from the IVIM model. Therefore, both an IVIM model and imaging parameters that can reliably detect the amount of non-Gaussian diffusion is required to reflect its dependence on the measured changes in shear stiffness.

The purpose of this study was to investigate the effect of the IVIM model and the number of b-value on accurate calculation of the virtual MRE.

Methods and materials

This study involved 39 patients with several liver diseases and after obtaining written informed consent, all patients underwent an MR examination including conventional MRE and diffusion-weighted image (DWI) sequence (see Table 1). In the DWI sequence, 27 patients and 12 patients were scanned using 3 and 5 b-value, respectively.

Three b-values (n=27)		Five b-values (n=12)	
n	Diagnosis	n	Diagnosis
8	Fatty Liver	2	Hepatitis B
4	NAFLD	2	Hepatitis C
4	NASH	2	Chronic hepatitis
2	HCC	2	NASH
2	Hepatitis B	1	NAFLD
2	Hepatitis C	1	HCC
5	Other	2	Other

Table 1
References: - Tokushima-shi/JP

MR imaging

1. MRE protocol

An external driver device (60 Hz) was used to induce shear waves in the liver tissue, and axial imaging of the abdomen with breath-holding was performed for conventional MRE. Imaging parameters were repetition time (TR), 33.3 ms; echo time (TE), 22.1 ms; flip angle, 30 degrees; field of view, 256 × 256; matrix size, 256 × 256; and slice thickness, 8 mm. Next, shear stiffness maps were generated using a multi-scale direct inversion algorithm on the MRI equipment.

2. DWI protocol

In addition, DWI with a fat-suppressed spin-echo echo-planar sequence was performed with the following parameters (see Table 2): TR, 12000 ms; TE, 89 ms; flip angle 30 degrees; matrix size, 256 × 256; slice thickness, 5 mm; and b-values, 0, 50, 200, 800, and 1500 s/mm^2. For b-value, data acquisition was performed separately for each three (0, 200, and 1500 s/mm^2) and five b-value (0, 50, 200, 800, and 1500 s/mm^2). For the patient DWIs acquired with the three and the five b-values, a number of excitations (NEX) were

applied to each b-value to improve the signal-to-noise ratio (SNR) of the DWI. In three b-value, one, two, and four of NEX were selected as 0, 200, and 1500 s/mm^2, respectively. In five b-values, one of NEX value was selected at 0-800 s/mm^2 of the b-values, and three NEX values were used at only 1500 s/mm^2 of the b-value. Here, all imaging parameters and setting value are shown in Table 2.

Data processing

In this study, Vitrea® software (Canon Medical Systems Corporation, Tochigi, Japan) and in-house software were used to generate several calculated maps (Matlab R2015b; MathWorks). The illustration of procedure of the experiments are shown in Figure 1. Shear stiffness of tissues of each of the patients was calculated from the conventional MRE data (see Figure 1a). Two *ADC* maps, which have different diffusion components, such as fast and slow diffusion components, were calculated from a slope of the DW signal attenuation between two b#values ($ADC_{0\#200}$ s/mm^2, $ADC_{200\#1500}$ s/mm^2) for each three and five b-value. Moreover, $ADC_{0\text{-}1500}$ s/mm^2, *D*, *D**, and # map were calculated from fitted signal attenuation curves with mono#exponential, bi#exponential, and stretched#exponential models using Bayesian fitting algorithms (see Figure 1b). All estimated parameter maps are represented as follows:

1. Two *ADC* maps derived from the slow and fast diffusion components without the non-least square method.

$$ADC_{0-200} = \ln\left(\frac{S_{b0}}{S_{b200}}\right) / \ 200 \quad \cdots \quad Eq1$$

Fig. 1: Eq.1
References: - Tokushima-shi/JP

$$ADC_{200-1500} = \ln\left(\frac{S_{b200}}{S_{b1500}}\right) / \ 1500-200 \quad \cdots \quad Eq2$$

Fig. 2: Eq.2
References: - Tokushima-shi/JP

where *S* is the DW signal and subscripts b_0-b_{1500} indicate *b*-values. In particular, $ADC_{200\text{-}1500}$ is more sensitive than $ADC_{0\text{-}200}$ with respect to the shear elasticity of the biomaterials [5].

2. The estimated parameter maps for each of the IVIM models with non-least square method using the Bayesian fitting algorithm.

a. mono-exponential

$$\ln\left(\frac{S}{S_0}\right) = -(b-b_0)\,ADC \quad \cdots \quad Eq3$$

Fig. 3: Eq3
References: - Tokushima-shi/JP
b. bi-exponential

$$\ln\left(\frac{S}{S_0}\right) = f\,exp[-bD^*]+(1-f)\,exp[-bD] \quad \cdots \quad Eq4$$

Fig. 4: Eq.4
References: - Tokushima-shi/JP

c. stretched exponential

$$\ln\left(\frac{S}{S_0}\right) = \{-(-b-b_0)DDC\}^{\alpha} \quad \cdots \quad Eq5$$

Fig. 5: Eq.5
References: - Tokushima-shi/JP
where, the *b* and *b0* are the b-values of the desired value and 0 s/mm^2. In this study, 0, 50, 200, 800, and 1500 s/mm^2 of the b-values were used. An illustration of experimental procedure is shown in Figure 1.

Data statistics

A region of interest (ROI) analysis was performed for each patient and was placed on the liver of # map avoiding unwanted signals, such as a large vessel region for each three and five b-value (see Figure 1c). In this study, threshold values were applied to each of the estimated parameters to remove the component of inhomogeneous signal variance caused by the vessels, low SNR, and other imperfections in the liver, as shown in Figure 1d. For the # map, the threshold values were determined from # ($0.01 < \# < 1$). $ADC_{0\text{-}200}$ and $ADC_{200\text{-}1500}$, a threshold of less than 0.025 mm^2/s was then used to remove unwanted *ADC* signals. No threshold was used for the *D** and *D* values in this study. After removing unwanted signals in the ROI, linear regression for each of the patients was applied to the conventional shear stiffness against the estimated parameter map of the IVIM model on the ROI. Outliers of the mean value were systematically excluded for each of the linear regression results (see Figure 1e). Finally, the IVIM maps were empirically converted to virtual shear stiffness from the results of linear regression with the removed the outliers (see Figure 1f).

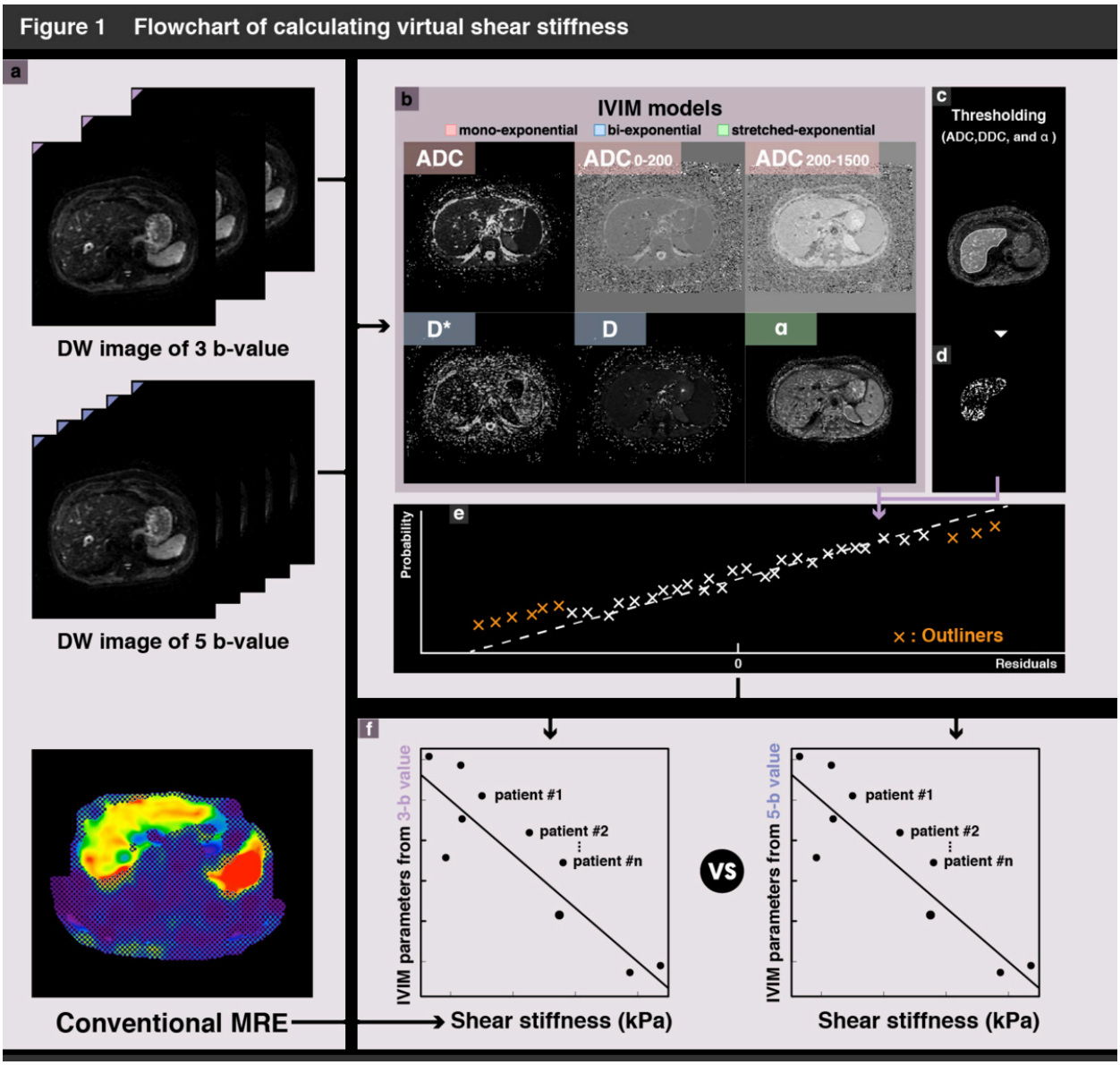

Fig. 6
References: - Tokushima-shi/JP

Results

The results of this study are indicated in Figure 2 and 3.

The signal attenuation derived from the three b-values, $ADC_{0\text{-}1500}$ and D^* against the measured shear stiffness, showed good correlation in comparison to that from the use of five b-values. In the fast diffusion component of three b-value, D^* resulted in good correlation while there was no correlation on the $ADC_{0\text{-}200}$. There was no correlation between the measured shear stiffness and the slow diffusion component, the $ADC_{200\text{-}1500}$, and D.

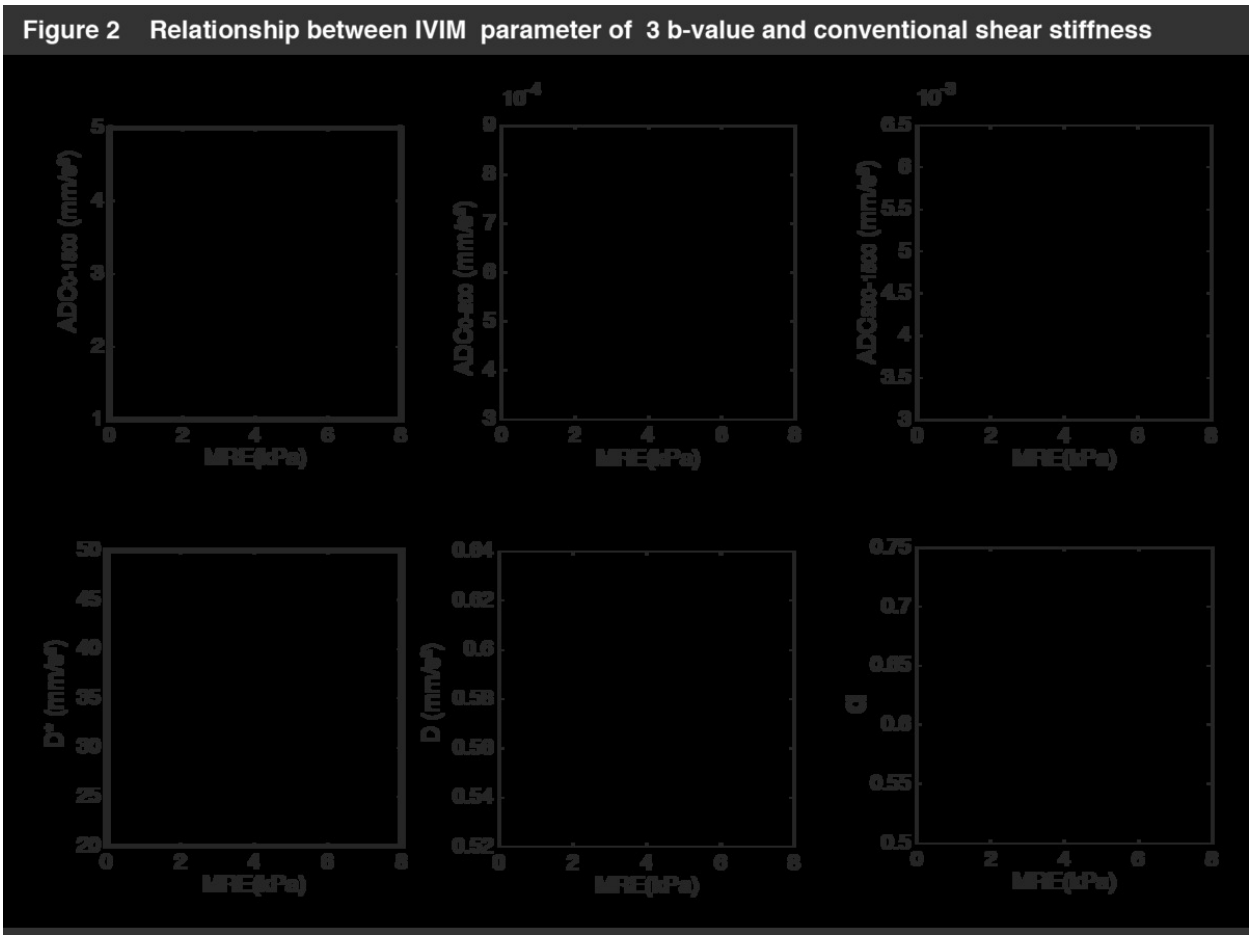

Fig. 7
References: - Tokushima-shi/JP

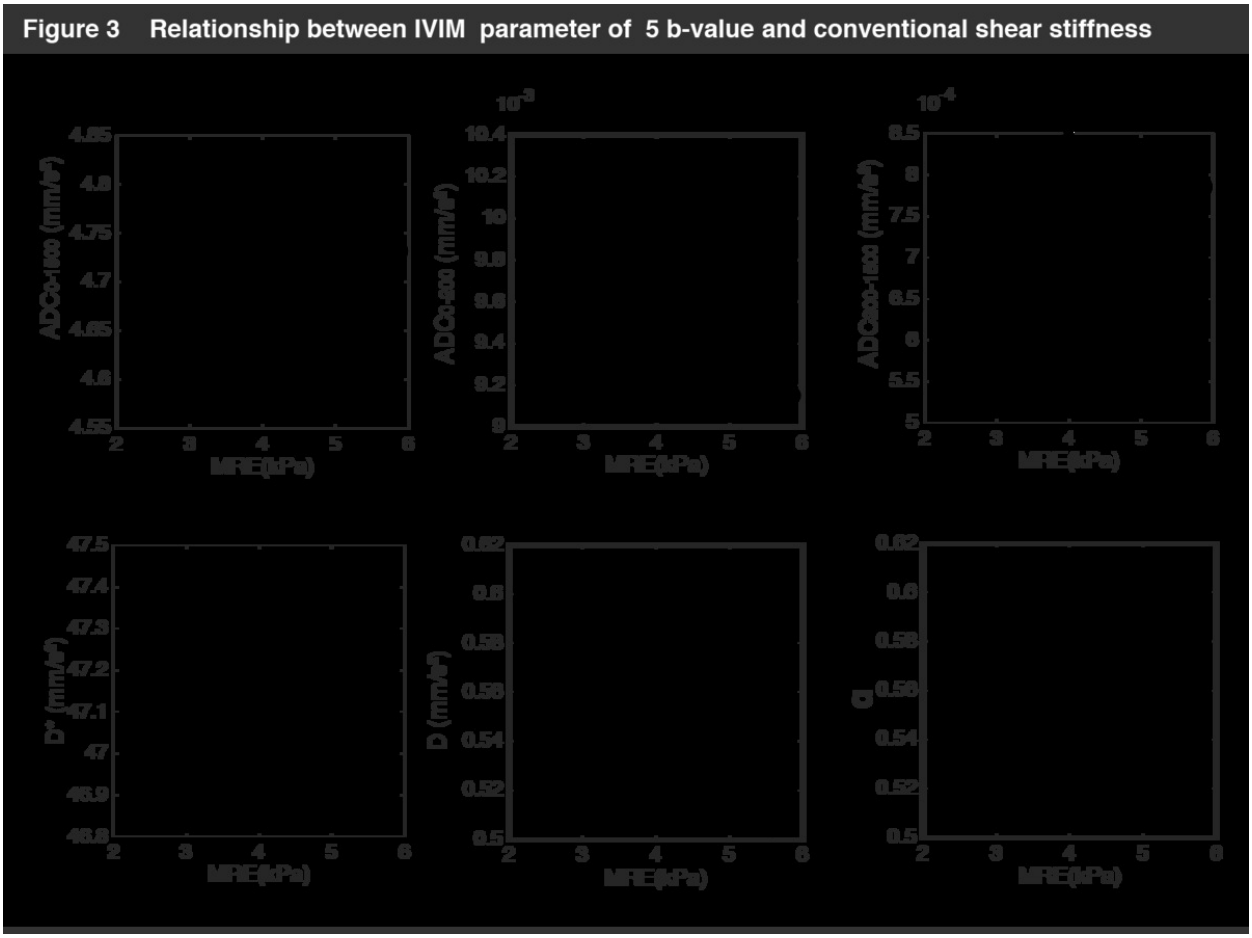

Fig. 8
References: - Tokushima-shi/JP

In each of the results from the linear regression of the estimated parameter maps calculated from the five b-value, a significant correlation, (R< #0.67), was observed between $ADC_{0\#200}$, D, and #, and the measured shear stiffness.

In addition, the relationship between the D and the measured shear stiffness had the best correlation for five b-value in this study (R=-0.8).

Normal 0 10 pt 0 2 false false false EN-US JA X-NONE

Moreover, the comparison between conventional shear stiffness and virtual shear stiffness is shown in Figure 4 and 5, demonstrating a correlation on each of the estimated parameters.

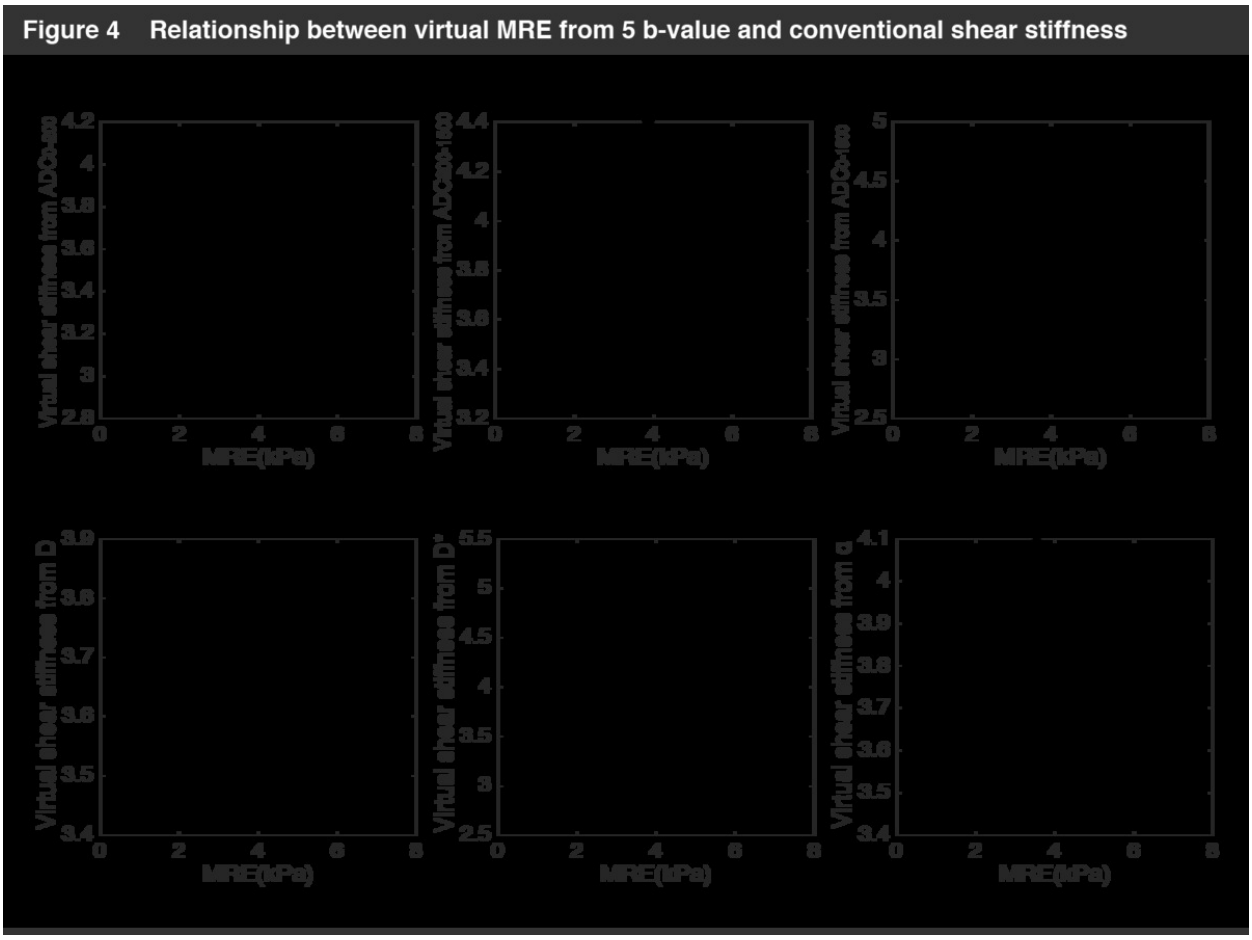

Fig. 9
References: - Tokushima-shi/JP

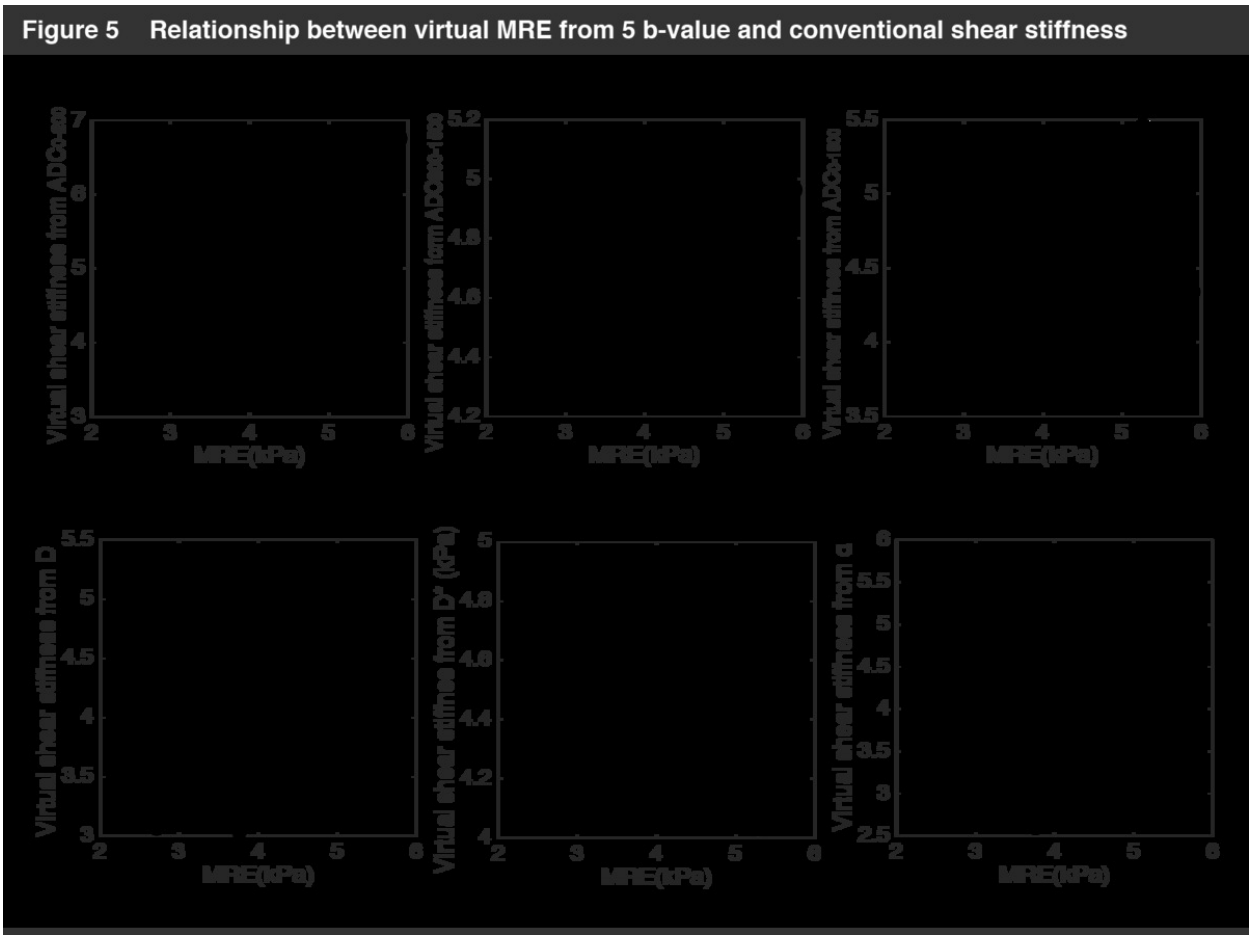

Fig. 10
References: - Tokushima-shi/JP

Conclusion

The purpose of this study was to investigate the effect of the IVIM model and the number of b-value on accurate calculation of the virtual MRE. In this study, the results of the linear regression between the estimated IVIM parameter map and the measured shear stiffness depended on IVIM models and the number of b-value. The result suggest that the estimated IVIM parameter map not only has information about the shear stiffness obtained from non-Gaussian diffusion, but also contains several factors which are unwanted for the virtual MRE. Thus, these unwanted factors in the base images, used to calculate virtual shear stiffness such as the *ADC*, *D**, *D* and # map, should be taken into consideration. For example, the probability distribution function (PDF) of the base images is important and when the SNR of the base image is inadequate, the PDF in the liver is described by a Rayleigh distribution and becomes asymmetric [12, 13]. The mean and mode of the PDF are thus not consistent in this asymmetric distribution as shown in figure 9.

Several factors may have influenced the result of the virtual MRE. Therefore, a robust method, which can separate the non-Gaussian diffusion having component of shear stiffness of the liver tissue, is needed for virtual MRE.

References

1. Yin M, Talwalkar JA, Glaser KJ et al (2007) Assessment of hepatic fibrosis with magnetic resonance elastography. Clin Gastroenterol Hepatol. 5:1207-1213

2. Bell H, Jahnsen J, Kittang E, Raknerud N, Sandvik L (2004) Long-term prognosis of patients with alcoholic liver cirrhosis: a 15-year follow-up study of 100 Norwegian patients admitted to one unit. Scand J Gastroenterol. 39:858-63

3 Muthupillai R, Lomas DJ, Rossman PJ, Greenleaf JF, Manduca A, Ehman RL (1995) Magnetic resonance elastography by direct visualization of propagating acoustic strain waves. Science. 269:1854-7

4. Huwart L, Sempoux C, Vicaut E et al (2008) Magnetic resonance elastography for the noninvasive staging of liver fibrosis. Gastroenterology. 135:32-40

5. Le Bihan D, Ichikawa S, Motosugi U (2017) Diffusion and Intravoxel Incoherent Motion MR Imaging-based Virtual Elastography: A Hypothesis-generating Study in the Liver. Radiology. 285:609-619

6. Le Bihan D, Breton E, Lallemand D, Grenier P, Cabanis E, Laval-Jeantet M (1986) MR imaging of intravoxel incoherent motions: application to diffusion and perfusion in neurologic disorders. Radiology. 161:401-7

7. Clark CA, Le Bihan D (2000) Water diffusion compartmentation and anisotropy at high b values in the human brain. Magn Reson Med. 44:852-9

8. Sehy JV, Ackerman JJ, Neil JJ (2002) Evidence that both fast and slow water ADC components arise from intracellular space. Magn Reson Med. 48:765-70.

9. Bennett KM, Schmainda KM, Bennett RT, Rowe DB, Lu H, Hyde JS (2003) Characterization of continuously distributed cortical water diffusion rates with a

stretched-exponential model. Magn Reson Med. 50:727-34

10. Ichikawa S, Motosugi U, Morisaka H et al (2015) MRI-based staging of hepatic fibrosis: Comparison of intravoxel incoherent motion diffusion-weighted imaging with magnetic resonance elastography. J Magn Reson Imaging. 42:204-10

11. Le Bihan D (2017). What can we see with IVIM MRI? Neuroimage. 1053-8119(17)31086-8

12. Henkelman RM (1985) Measurement of signal intensities in the presence of noise in MR images. Med Phys. 12:232-3

13. Gudbjartsson H, Patz S. The Rician distribution of noisy MRI data (1995) Magn Reson Med. 34:910-4